# Characteristic Parameters Extraction Method of Hidden Karst Cave from Borehole Radar Signal

Jinchao Wang[1]; Chuanying Wang[2]; Zengqiang Han[3]; Xianjian Zou[4]; Yiteng Wang[5]; Chao Wang[6]; and Sheng Hu[7]

**Abstract:** A hidden karst cave has a prominent influence on the design and construction of underground engineering. In order to improve the automatic identification accuracy of hidden karst cave areas and the acquisition accuracy of characteristic parameters in borehole radar signals, combined with the reflection characteristic relationship between radar electromagnetic waves and hidden karst caves, research methods on borehole radar image pre-processing and feature parameter extraction of hidden karst caves are carried out. First, based on the original signal of a borehole radar, the reflection characteristic relationship between the electromagnetic waves of the borehole radar and a hidden karst cave is established, and the geometric model of borehole radar detection of hidden karst caves is formed. Then, the reconstruction of borehole radar signals is realized by searching the peak position of Pmusic function combined with the subspace MUSIC method. Combining the continuity of hyperbola and the gray level difference of a nonreflective region, an improved variance method is proposed, which is more suitable for the actual borehole radar image segmentation. It realizes the suspected hidden karst cave inversion by setting a threshold of continuous pixels, a simultaneous gradient operator, and a maximum interspecific variance method. Finally, according to the geometric model of borehole radar detection, the energy-weighted fitting of a hyperbolic profile is carried out, and the improved Hough transform method is used to solve the multiple characteristic parameters of the hyperbolic model, so as to extract the characteristic parameters of the hidden cave from the borehole radar signal. The example analyzed proves that the method is feasible and accurate, which can provide important data support for underground engineering.
**DOI:** 10.1061/(ASCE)GM.1943-5622.0001733. 

**Author keywords:** Borehole radar; Hidden cave; Edge detection; Cave scale; Dielectric constant.



## Introduction

With the rapid development of a global society and economy, the infrastructure construction scale of highways, railways, and large-scale buildings in various countries is constantly expanding. A large number of projects under construction and planning will inevitably encounter adverse geological structures, such as uneven soft and hard bottom, fragmentation, solitary rocks, shallow overburden of water, and underground karst caves. Hidden karst caves have a more prominent impact on engineering design and construction. If we cannot find out whether there are hidden karst caves in the underground ahead of time, serious hidden safety hazards will be buried, possibly causing casualties, delays in the construction period, and major economic losses (Li 2015; Su et al. 2007; Li et al. 2011). In order to perform underground engineering construction smoothly and safely through the distribution area of hidden karst caves, it is particularly important to detect these hidden caves in advance, to analyze them according to the results of detection, and to evaluate their adverse effects on the construction process through the distribution area of the hidden caves (Cheng et al. 2018, 2019). Ground-penetrating radar is a fast, nondestructive, and high-resolution detection method that is very sensitive to aquifers. Ground-penetrating radar is very suitable for the detection of hidden caves (Zeng et al. 2010; Liu and Qian 2015; Li et al. 2014). However, common ground-penetrating radar is not suitable for deep stratum structure detection because of the detection depth limitation. In order to obtain the structure information of deep stratum directly, boreholes are often drilled, but because of the "one hole view," it is easy to miss the source of a disaster. In order to solve these problems, an antenna can be placed in the existing borehole to detect the occurrence of hidden karst caves in a certain range around the borehole, which can effectively solve the problems of limited detection depth and the "one hole view" of general geological radar. Therefore, borehole radar has been widely used in the detection of hidden karst caves (Slob et al. 2010; Liu 2002; Wu et al. 2008; Jiao et al. 2019).

The electromagnetic wave of a borehole radar will reflect when it passes through the medium interface of different dielectric constants, and can be used to detect a hidden cave on the outer perimeter of the drilling, however, the traditional radar interpretation

[1]Assistant Research Fellow, State Key Laboratory of Geomechanics and Geotechnical Engineering, Institute of Rock and Soil Mechanics, Chinese Academy of Sciences, Wuhan 430071, China (corresponding author). Email: jcwang@whrsm.ac.cn

[2]Research Fellow, State Key Laboratory of Geomechanics and Geotechnical Engineering, Institute of Rock and Soil Mechanics, Chinese Academy of Sciences, Wuhan 430071, China.

[3]Associate Research Fellow, State Key Laboratory of Geomechanics and Geotechnical Engineering, Institute of Rock and Soil Mechanics, Chinese Academy of Sciences, Wuhan 430071, China.

[4]Assistant Research Fellow, State Key Laboratory of Geomechanics and Geotechnical Engineering, Institute of Rock and Soil Mechanics, Chinese Academy of Sciences, Wuhan 430071, China.

[5]Assistant Research Fellow, State Key Laboratory of Geomechanics and Geotechnical Engineering, Institute of Rock and Soil Mechanics, Chinese Academy of Sciences, Wuhan 430071, China.

[6]Doctoral Student, State Key Laboratory of Geomechanics and Geotechnical Engineering, Institute of Rock and Soil Mechanics, Chinese Academy of Sciences, Wuhan 430071, China.

[7]Senior Engineer, State Key Laboratory of Geomechanics and Geotechnical Engineering, Institute of Rock and Soil Mechanics, Chinese Academy of Sciences, Wuhan 430071, China.

Note. This manuscript was submitted on August 18, 2019; approved on January 30, 2020; published online on May 21, 2020. Discussion period open until October 21, 2020; separate discussions must be submitted for individual papers. This paper is part of the ***International Journal of Geomechanics***, © ASCE, ISSN 1532-3641.

process is more cumbersome (Zhong et al. 2017). In order to extract the effective information of the borehole radar signal more fully, it is of great significance to create a set of techniques and methods that can automatically identify and distinguish hidden caves. A hidden cave in the complete surrounding rock belongs to the electrical mutation point, the electromagnetic wave reflects in the boundary of the hidden cave, forming a curved reflection wave with strong amplitude, and often shows a double curve on the borehole radar time profile, which is a prior knowledge in the two-dimensional echo image of the borehole radar. However, for the hyperbolic features existing in the borehole radar image, there is no specific interpretation model, thus it is difficult to directly extract the hidden cave feature parameters that are useful for engineering design and construction, such as position, scale, and dielectric constant of the rock layer (Li et al. 2017; Xu et al. 2018; Perrotti et al. 2018), for the borehole radar detection of hidden-cave technology. It is therefore urgent that a method for extracting the characteristic parameters of hidden caves is proposed.

In view of the common problems of borehole radar detection of hidden caves, this paper based on the original signal of borehole radar establishes the reflection characteristic relationship between the borehole radar electromagnetic wave and the hidden cave, and forms the geometric model of the hidden cave borehole radar detection, and combines the subspace MUSIC method to realize the reconstruction of the borehole radar signal. In the aspect of radar signal reconstruction and feature curve extraction, in order to sharpen the hidden cave reflection feature area, better realized image segmentation combined with the hyperbole has certain continuity characteristics in curve edge detection, setting a continuous pixel threshold to achieve the suspected hidden cave feature extraction in radar signal image. In the aspect of the hidden cave feature parameters extraction, according to the geometric model of borehole radar detection, the energy-weighted fitting of the hyperbolic contours is used to solve several characteristic parameters of the hyperbolic model by the improved Hough transformation method, so as to extract the hidden cave feature parameters of the borehole radar signal. This method is analyzed and verified by the practical engineering.

## Borehole Radar Signal Response of Hidden Karst Cave

In order to simplify the hidden cave model, the pattern of the hidden cave is analyzed by the point-shaped geological body model to identify the structural characteristics of the hidden cave, and the electromagnetic wave of the borehole radar propagates in the soil medium containing the hole or other point-like hidden cave, as shown in Fig. 1. The outer area of the hidden cave is the geotechnical medium, assuming that the hidden cave is the standard circle. We established a right-angle coordinate system with the center point of the bore hole as the center of the circle and the vertical downward direction as the positive direction of the $y$-axis. The center coordinates of the hidden cave A is $(x_0, y_0)$. The radius of the hidden cave is recorded as $r$, and the point D is the reflective point position of the radar electromagnetic wave on the hidden cave. At this time, the electromagnetic wave emitted by the transmitting antenna $T$ is received by the receiving antenna $R$, and the electromagnetic wave travel distance l is the sum of TD and DR. It should be noted that the antenna used in the borehole radar is a antenna of receive emit common probe, which moves in the direction of the drilling and emits a broadband high-frequency pulse around the borehole. Because the mechanism of radar electromagnetic wave propagation in rock and soil is very complex, in order to discuss the problem conveniently, it is assumed that the underground medium is uniform and nondispersive, and ignores the Fresnel diffraction effect of the borehole wall and the reflection of electromagnetic waves when the air enters the ground.

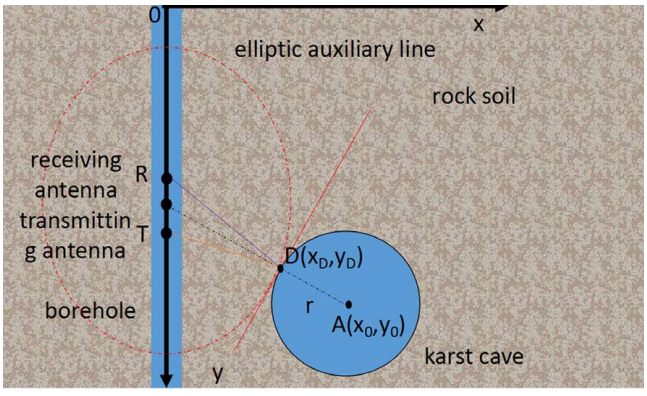


**Fig. 1.** Simplified model of hidden cave borehole radar detection.

According to the standard equation of the circle, the boundary equation of the hidden cave can be seen (Zhong 2008), and the tangent equation of the circle over the point D $(x_D, y_D)$ is

$$(x - x_0)(x_D - x_0) + (y - y_0)(y_D - y_0) = r^2 \tag{1}$$

If the antenna distance TR is known to be $d$, the detection depth of the borehole radar is OR, with $R$ and $T$ as the focus as an auxiliary ellipse line and round A tangent to the point D, the elliptical tangent equation of the D-point can be known as

$$\frac{x_D x}{a^2} + \frac{(y_D - \mathrm{OR} - d/2)(y - \mathrm{OR} - d/2)}{b^2} = 1 \tag{2}$$

The tangent of circle A and the elliptical RT is the same line, and since the point D $(x_D, y_D)$ is on the circle A and the elliptical RT, it is joined together:

$$\begin{cases} \left(\dfrac{x_0}{a^2 k_0 - 1}\right)^2 + \left(\dfrac{y_0 - \mathrm{OR} - d/2}{b^2 k_0 - 1}\right)^2 = r^2 \\ \dfrac{a^2 k_0^2 x_0^2}{(a^2 k_0 - 1)^2} + \dfrac{b^2 k_0^2 (y_0 - \mathrm{OR} - d/2)^2}{(b^2 k_0 - 1)^2} = 1 \\ \dfrac{x_D^2}{a^2} + \dfrac{(y_D - \mathrm{OR} - d/2)^2}{b^2} = 1 \end{cases} \tag{3}$$

The relationship formula Eq. (3) can be solved by numerical method $a$, $bi$, and $k_0$ parameters of numerical solution. Antenna distance TR in this case is small enough, so the antenna distance on the propagation distance can be ignored, at this time, thus making it is easy to find the radar electromagnetic wave propagation distance l, which can be represented as

$$l = 2\sqrt{x_0^2 + (y_0 - (\mathrm{OR} + d/2))^2} - 2r \tag{4}$$

This can be expanded to achieve

$$\frac{(l + 2r)^2}{4x_0^2} - \frac{(y_0 - \mathrm{OR} - d/2)^2}{x_0^2} = 1 \tag{5}$$

If $y = \mathrm{OR} + d/2$, the detection point position of the borehole radar is $y$, then the relational Eq. (5) can be rewritten to a hyperbolic equation about $l$ and $y$, with the expression:

$$\frac{(l + 2r)^2}{4x_0^2} - \frac{(y - y_0)^2}{x_0^2} = 1 \tag{6}$$

As can be seen from the previous discussion, when the borehole radar is used for hidden cave detection, if the hidden cave is

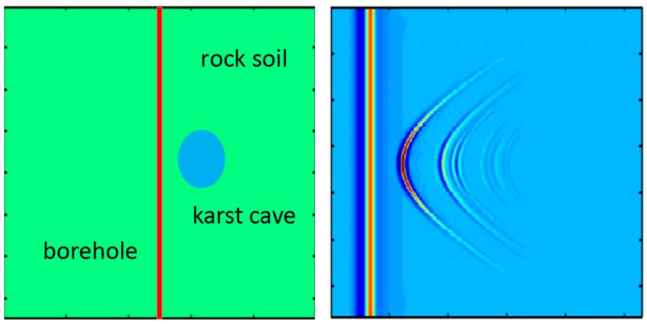


**Fig. 2.** Model and its radar response map: (a) hidden cave model; and (b) borehole radar response.



encountered in the outer perimeter of the drilling, in the B-Scan image composed of multichannel scanning data, the target echo is multicurved or approximate layover geometry, determined by the radar motion and the geometry of the relative distance change of the target. The transmission distance of radar electromagnetic waves can be obtained from the speed of transmission of the electromagnetic waves and the delay of the echo, so that the relationship type in Eq. (6) can be rewritten as

$$\frac{t^2}{t_0^2} - \frac{4(y-y_0)^2}{v^2 t_0^2} = 1 \tag{7}$$

The relational type in Eq. (7) is the three-parameter hyperbolic model of the energy space distribution of the borehole radar echo, where $v$ = the speed of transmission of radar electromagnetic waves in the geotechnical medium; $y_0$ = the horizontal coordinate of the hidden cave; $t_0$ = the horizontal coordinate of the hidden cave position in the Y–T plane, corresponding to the hidden cave away from the drilling distance $d_0 = vt_0/2$. The echo hyperbole of the hidden cave in the B-Scan image, which is composed of the multichannel scan data, can be uniquely determined by the vertex coordinates ($y_0$, $t_0$), the eccentricity $e = v/2$. Fig. 2 shows the simulation diagram.

## Radar Signal Reconstruction and Feature Curve Extraction

### *Borehole Radar Signal Reconstruction*

In borehole radar detection, the radar moves along the hole during detection, while the radar antenna transmits electromagnetic waves and records the echo signal, that is, the drilling B-Scan image is composed of multiway, one-dimensional radar signals. However, the clutter signal will shield or bury the deep or complex target signal in the actual detection, and the noise reduction process of the Fourier leaf space can be used to improve the signal-to-noise ratio of the radar signal image by studying the statistical characteristics of the noise signal smoothness. When setting $V = [v_1, v_2, v_3, \ldots, v_m]$ as the signal subspace, $v_i$ = a subspace vector, whose vectors are linearly independent, and $m$ = the set number of subspaces. Hence, the borehole radar echo signal can be expressed as the sum of the weighted subspace base vectors, which are expressed as

$$s = \sum_{i=1}^{m} a_i v_i \tag{8}$$

In the one-dimensional radar signal of the hidden cave, the signal can be decomposed into three subspaces of useful target body, clutter, and noise. Subspace decomposition is intended to preserve the signal subspace, eliminating noise and clutter. Compared with the target reflective signal, the clutter energy is generally relatively small, but in the process of de-clutter interference, the coherent signal is processed using spatial smoothing, thus suppressing multiple wave interference and improving the ability of weak characteristic signal extraction.

In the radar algorithm, the multiple signal classification (MUSIC) method can improve the resolution of the arrival direction and has a good application effect in determining spatial position. The MUSIC method uses the orthogonality of both signal and noise subspace to construct a spatial spectrum function, and detects the direction of the signal arrival through a spectrum peak search in order to improve the spatial position, which can determine the accuracy. Therefore, this paper uses the MUSIC method to estimate the location of hidden karst caves. By setting the reflection factor of a one-dimensional scan line of the borehole radar to $L$ (1, 2, 3, …$L$), $L < M$, the position of the hidden cave is determined by the super-resolution peak point of the subspace. The exact position of each signal reflection point is estimated by searching for the peak point position of the MUSIC function (Pmusic), which is expressed as (Odendaal et al. 1994)

$$P_{\text{music}(\tau)} = \frac{1}{\alpha(\tau)^H E_N E_N^H \alpha(\tau)} \tag{9}$$

where $\alpha(\tau)$ = the time-lapse vector of the target reflected signal, indicating the position depth of the underground hidden cave; $E_N$ = an $L\times$ ($L$-$k$) residual matrix that contains a characteristic vector with clutter and noise ($L$-$k$). As can be seen in Fig. 3(a), the envelope in the receiving signal radar echo chart has multiple waves, clutters and noise. Through the subspace MUSIC method, the various signals received by the radar are projected into different subspaces, so as to suppress unwanted interference signals and effectively extract useful information, while the clutter and multiple waves are almost completely removed. The results are shown in Fig. 3(b).

### *Feature Curve Extraction*

Borehole radar image in the process of generation and transmission is often disturbed and influenced by various noise sources that make the image worse, noise makes the original uniform and a continuous change of grayscale can suddenly become larger or reduced, forming some false object edges or contours. In addition, disturbance by various noise sources is often expressed as isolated pixels, similar to snowflakes, which make the image contaminated. Therefore, it is necessary to suppress or eliminate this kind of noise and improve the image quality of the borehole radar. Because

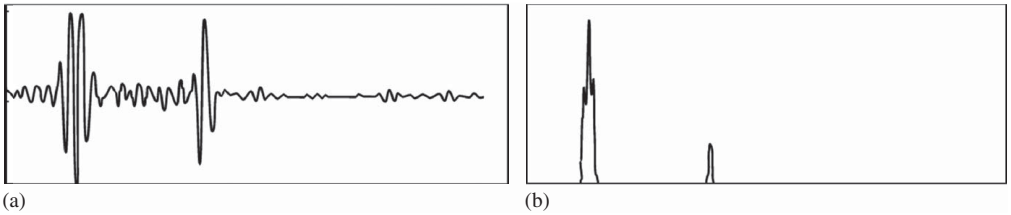

**Fig. 3.** Radar one-dimensional wave and MUSIC analysis: (a) one-dimensional waveform; and (b) MUSIC search spectrum.

adaptive median filtering can effectively preserve the edge features of the image, this paper selects the adaptive median filtering method for image de-drying.

The principle of adaptive median filtering is to adjust the size of the filter window by noise density, and to process the noise points and signal points by different treatment methods. The noise points are then filtered at the median, keeping the grayscale value of the signal points unchanged. The grayscale value of the pixel point $(x, y)$ in the drill radar image is $f_{xy}$, the current working window is represented by $K_{xy}$, the preset allowed maximum window is represented by $K$, and the grayscale minimum, median, and maximum value is respectively set in $f_{\min}, f_{\text{med}}, f_{\max}$. The basic steps of the algorithm are as follows:

1. If $f_{\min} < f_{\text{med}} < f_{\max}$, go to step (2), or increase the window $K_{xy}$ size. If the size of $K$ is smaller than the size of $K_{\max}$, repeat step (1) or the output is $f_{xy}$.
2. If $f_{\min} < f_{xy} < f_{\max}$, the output is $f_{xy}$, or the output is $f_{\text{med}}$.

In the adaptive median filtering algorithm, the detection and determination of noise points is based on $f_{\min}$ and $f_{\max}$, and when $f_{\min} < f_{\text{med}} < f_{\max}$, it is shown that $f_{\text{med}}$ is not noise, thus judging whether $f_{xy}$ is noise based on $f_{\min} < f_{xy} < f_{\max}$. If neither $f_{xy}$ nor $f_{\text{med}}$ is pulse noise, priority output is $f_{xy}$. Fig. 4 shows the contrast chart before and after adaptive median filtering.

After completing the adaptive median filtering of the drill edited radar image, the grayscale and color variation information of the image needs to be completely discarded, leaving only a shape area consisting of black or white pixels containing most of the shape information of the target. If the traditional image segmentation method causes information interference or missing feature information (Wang et al. 2017), there are certain characteristics of difference required in order to sharpen the hidden cave reflection feature area and better realize image segmentation (according to the hidden cave reflection feature curve and the grayscale value of nonfeatured area in the borehole radar image). The gradient operator algorithm is combined with the largest class variance method to divide the image, with the gradient being used to represent the discontinuity at the edge of the hidden cave reflection feature curve, so as to achieve a sharpening of the feature curve. A borehole radar image is defined as a two-dimensional function $f(x, y)$ whose gradient is defined as

$$\nabla f = \text{grad}(f) = \begin{bmatrix} G_x \\ G_y \end{bmatrix} \tag{10}$$

where $G_x$ and $G_y$ = the approximate first-order derivative. The magnitude value is

$$|\nabla f(x, y)| = \sqrt{G_x^2 + G_y^2} \tag{11}$$

The concrete implementation steps are: the de-noise processing of the borehole radar image $F_1$ gradient processing, the formation of gradient image $F_2$, $F_2$ for two-value, obtain two-value image $F_3$, and then the image $F_1$ and $F_3$ two-dimensional array corresponding points multiplied to obtain a new image $F_4$. Finally, the largest interclass variance processing image $F_4$ achieve threshold $T$, which is the best threshold for image $F_1$. If the pixel value of the borehole radar image $F_1$ is set to 1, that is, white, this represents the background information, and if the pixel value less than or equal to the best threshold $T$ is set to 0, that is, black, it represents the feature information. Fig. 5 shows the comparison of the borehole radar two-value effect with the largest class variance method by this method.

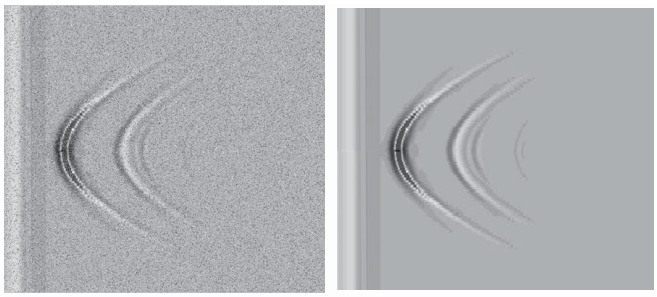

**Fig. 4.** Contrast diagram of adaptive median filtering: (a) before filtering processing; and (b) after filtering processing.

### *Feature Curve Equation Fitting*

In order to achieve the equation fitting of the feature curve, it is necessary to obtain the edge profile information of the feature curve in the borehole radar image. Hough transformation is a method of organizing data in the global scope of the image using a model-based control strategy, which needs to establish a precise parametric equation for the selected type of target, and then transform the data from the image space to the defined parameter space, and the result of the parameter space accumulation is evidence of the target existence in the original space. One of the outstanding advantages of this method is that the test results are robust, that is, the loss of data and noise is not very sensitive, the disadvantage is that its calculation is large, and real-time is not strong. The relational hyperbolic Eq. (7) can be rewritten in the following form of a quadratic function:

$$g(y) = t^2 = p_0 + p_1 y + p_2 y^2 \tag{12}$$

Among them

$$\begin{bmatrix} p_0 \\ p_1 \\ p_2 \end{bmatrix} = \begin{bmatrix} t_0^2 + 4y_0^2/v^2 \\ -8y_0/v^2 \\ 4/v^2 \end{bmatrix} \tag{13}$$

At this point, the fit of the hidden cave echo hyperbolic curve becomes a typical secondary curve fitting problem, which can be resolved by the least square method, and the $y_0$ and $v$ of the hyperbolic model can be obtained by fitting the result. In the traditional detection method (Gurbuz et al. 2012; Chen et al. 2004; Zhu 2009; Rappaport et al. 2007), based on Hough transformation, the two-dimensional echo data B-Scan = $B(y, t)$. The hidden

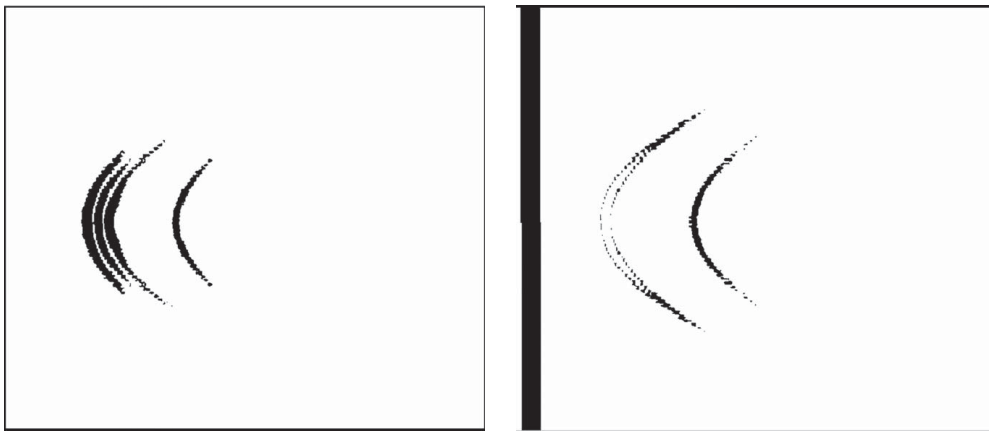

(a) (b)

**Fig. 5.** Borehole radar image two-value comparison: (a) maximum interclass variance; and (b) the method of this article.

cave hyperbolic $= C_{v,y_0,t_0}(y, t)$, and the $B(y, t)$ is added to realize Hough transformation:

$$H(\tilde{v}, \tilde{y}_0, \tilde{t}_0) = \sum_{(y,t)} B(y, t) \quad (y, t) \in C_{\tilde{v},\tilde{y}_0,\tilde{t}_0}(y, t) \tag{14}$$

Among them, $(\tilde{v}, \tilde{y}_0, \tilde{t}_0)$ that is, the three-dimensional parameter space of the $C_{v,y_0,t_0}(y, t)$ hyperbolic, when the Hough transformation results $H(\tilde{v}, \tilde{y}_0, \tilde{t}_0)$ a steep "peak" indicates the existence of a double curve $C_{v,y_0,t_0}(y, t)$. The detection of hidden cave can be achieved by locating $H(\tilde{v}, \tilde{y}_0, \tilde{t}_0)$ peaks, and the characteristic parameters of the hidden cave can be obtained by determining the parameters of the curve as follows:

$$(v_0, y_0, t_0) = \arg\max_{\tilde{v},\tilde{y}_0,\tilde{t}} |H(\tilde{v}, \tilde{y}_0, \tilde{t}_0)| \tag{15}$$

As can be seen from Eq. (15), the Hough transformation of B-Scan needs to be done directly in the three-dimensional $(\tilde{v}, \tilde{y}_0, \tilde{t}_0)$ parameter space of the hyperbolic, resulting in a large calculation. Detecting peaks from Hough transformation results, shows that $H(\tilde{v}, \tilde{y}_0, \tilde{t}_0)$ also faces the problem of parameter space, therefore, the traditional detection method based on Hough transformation raises the problem of computational efficiency, and after energy-weighted fitting, the two parameters $y_0$ and $v$ of the hidden cave echo hyperbolic model were estimated. Therefore, the Hough transformation only needed to be completed in a one-dimensional parameter space.

Similarly, a double curve $C_{v,y_0,t_0}(y, t)$ is indicated when $H(\tilde{t}_0)$ a steep "spike" occurs. The detection of the $H(\tilde{t}_0)$ peak can realize the detection of hidden cave, and the parameters of the hidden cave only need to finally determine the parameter $t_0$, because the Hough transformation and peak detection are carried out in the one-dimensional parameter space. Compared with the traditional Hough-based detection method, the calculation method of this paper will be significantly reduced as represented in the following:

$$t_0 = \arg\max_{\tilde{t}} |H(\tilde{t}_0)| \tag{16}$$

## Calculation and Analysis of Hidden Cave Feature Parameters

### *Hidden Cave Feature Parameters*

When there are hidden caves around the borehole, these are characterized by hyperbolic in the borehole radar B-Scan image composed of multiradar wave scanning data. As can be seen from the relational type Eq. (7), the target echo hyperbolic shape of the hidden cave is a function of the antenna moving position $y$, its B-Scan image schematic is shown in Fig. 6, where the $y$ axis represents the depth along the drilling direction, the $t$-axis represents the radar wave two-way walk. The measurement of dielectric constants can be carried out by using the relationship characteristics of the echo delay $t_n$ and the position $y_n$ of the borehole radar antenna.

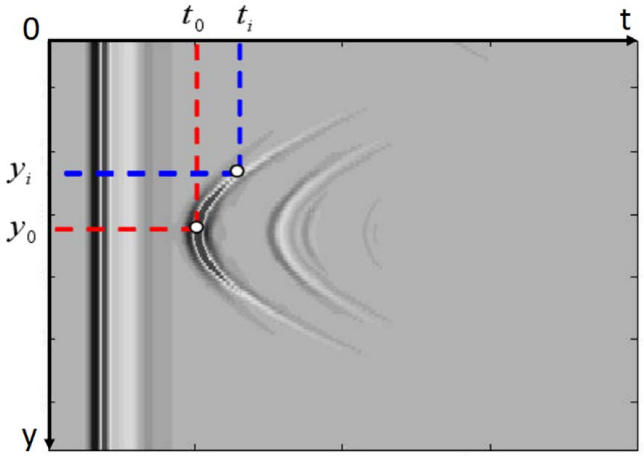


**Fig. 6.** A diagram of the hidden cave echo curve.

Assuming that the borehole radar is located on the right side of the hidden cave (i.e., the position of the drill edge radar corresponding to the hyperbolic vertex) is measured at $t_0$, and then the borehole radar is moved to the vertical distance of the hidden cave to measure the two-way travel time $t_1$, the relative dielectric constant $\varepsilon_r$ of the rock is

$$\varepsilon_r = c^2\sqrt{t_1^2 - t_0^2}/y^2 \tag{17}$$

where $c =$ the speed at which the electromagnetic wave propagates in the vacuum, and the first derivative of a point on the hyperbole $(y, \mathrm{t}(y))$ is

$$g(y_i) = \frac{dt_i}{dy_i} = \frac{4(y_i - y_0)}{v^2 t_i} \tag{18}$$

Assuming $u = v^2/4$, the upper formula can be written as $y = -g(y_i)t_i u + y_i$: all hidden cave echo curve points should satisfy

the relationship. Thus, the Hough algorithm can be transformed for each point in the point $S(t_0, x_0, v)$ set to

$$y_a = -g(y_i)t_i u_a + y_i \tag{19}$$

After each point transformation, a straight line in $\{x_a, u_a\}$ space is corresponding, wherein the line corresponding to the target echo curve should be exchanged at a point $(y_0', u)$ in the $\{x_a, u_a\}$ space, to search for the maximum peak point of the intersection overlay. The wave speed $v'$ can be estimated, and the target's exact position $(y_0', z_0')$ can be calculated, where $z_0' = t_0'/v'$. By bringing the point set $(t_i, y_i)$ into the relational (17) and the radius $r_i$ of the hidden cave can be deduced as

$$r_i = \left| \frac{v}{4}(t_i + t_0) + \frac{(y_i + y_0)^2}{v(t_i - t_0)} \right| \tag{20}$$

### Instance Analysis

In order to verify the feasibility and effectiveness of this method, the hidden cave borehole radar survey data along the subway section of the Bohai region was selected, the example analysis was carried out, and the borehole radar data acquisition was based on the SIR 200 borehole radar produced by GSSI Company, and the antenna frequency in the shielded hole attached to it was 100 MHz. In the radar waveform image of the drilling drill ZK26, the approximate hyperbolic profile appears at a position of about 30 m below the seabed, suspected to be a hidden cave reflective echo, and its borehole radar signal waveform is shown in Fig. 7(a). From Fig. 7(a), the borehole radar signal has a noise signal. In order to improve the signal-to-noise ratio of the radar signal image, by using the subspace MUSIC method, the one-dimensional waveform of the borehole radar signal is decomposed into three subspaces of the useful target body, clutter, and noise, and the clutter coherent signal is processed by using space smoothing to suppress multiple wave interference, and the reconstruction of the borehole radar signal is realized. From Fig. 7(b), shows that the borehole radar signal reconstruction by subspace MUSIC method, the image suppression obtained inhibits some interference signal, effectively highlighting the useful information.

In the process of detection, due to uneven geotechnical media and the presence of dispersion phenomenon, the attenuation of electromagnetic waves in the medium and a variety of coherent noise, random interference and many other factors, the result was a blurred hidden cave profile image where the hyperbole characteristics are not obvious, according to the previous description. In this paper, adaptive median filtering was selected to pre-process the borehole radar signal reconstruction map, and the results are shown in Fig. 8(a). Fig. 8(a) shows that the noise points existing in the borehole radar signal reconstruction map are effectively removed, and the image is more clear. In order to completely discard the grayscale and color variation information of the pre-processed image, according to the characteristics of the hidden cave reflection feature curve and the grayscale value of the nonfeatured area in the borehole radar image, the gradient operator is combined with the largest class variance method to divide the image, and obtain the two-value image of the borehole radar image. The results are shown in Fig. 8(b).

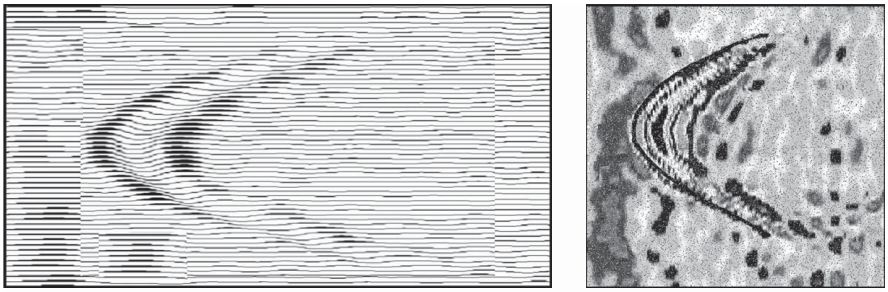

(a) (b)

**Fig. 7.** Original waveform and signal reconstruction: (a) raw borehole radar wave; and (b) borehole radar signal reconstruction map.

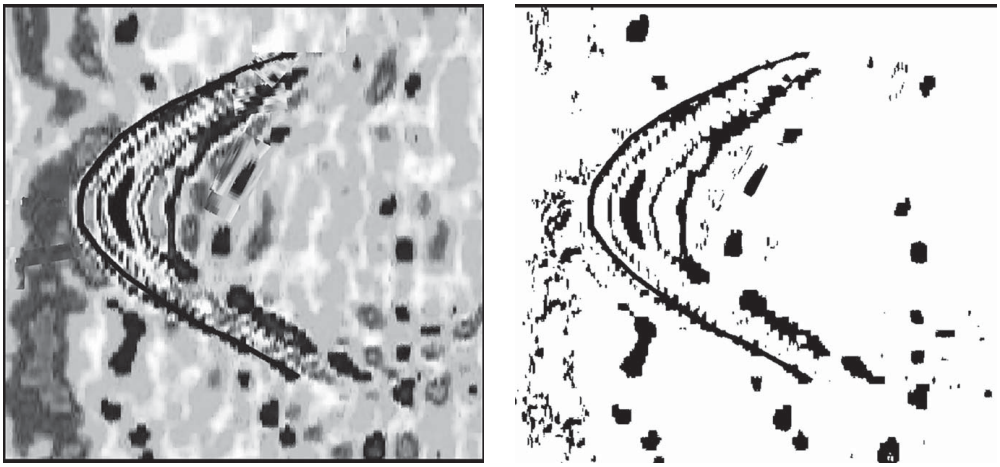

(a) (b)

**Fig. 8.** Borehole radar preprocessing diagram and binarization diagram: (a) borehole radar preprocessing map; and (b) borehole radar binary map.

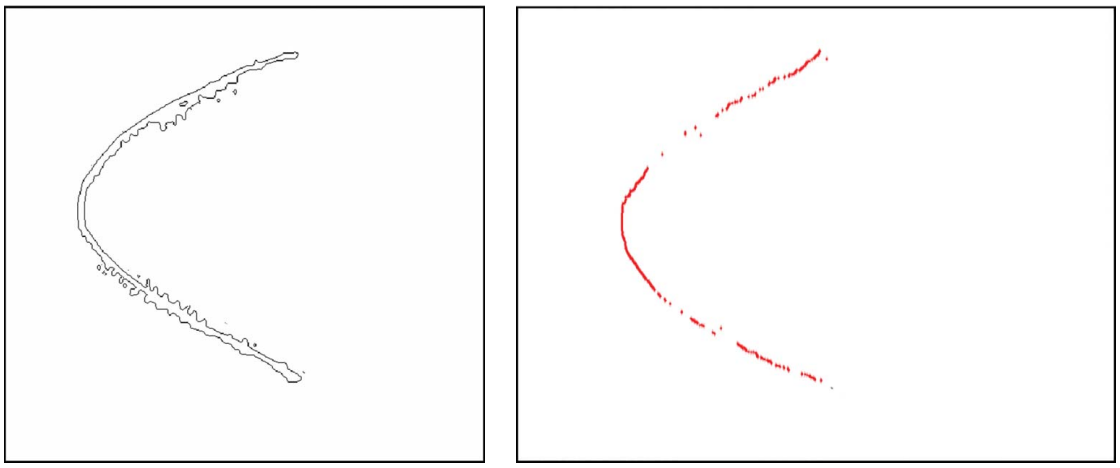


**Fig. 9.** Characteristic contours and characteristics of suspected hidden caves reflection curves: (a) hyperbolic characteristic contour; and (b) hyperbolic characteristic contour points.

As can be seen from Fig. 8(b), there are abnormal shape areas of the discontinuous curve class in the borehole radar binary map. In order to sharpen the hidden cave reflection feature area and better realize image segmentation, combined with the hyperbole of a certain continuity characteristics in the curve edge detection, we set the continuous pixel threshold. The hyperbolic contour extraction of the suspected hidden cave reflection feature was achieved. The results are shown in Fig. 9(a). In the acquisition of the hyperbolic feature contour point, the horizontal section scan is used to extract the midpoint of the outline, and the feature contour point is shown in Fig. 9(b).

In the hyperbolic equation fitting of the suspected hidden cave, the hyperbolic equation rendezvous based on the Hough transformation is used, and the specific processing steps are as follows:

1. To scan each row of data, if the cross-coordinate series within 1/4 of the data corresponding to the maximum number of times is the time reached by the direct wave, and then traversed all points in the range of 1/4 to 1/2, according to the hidden cave return peak tracking method to count the vertices in line with the hyperbole characteristics, save all the required vertices into the queue.
2. Empty all parameter lists, take out vertices in a queue, and exit if they have been all processed. Matching the upper support of the hyperbole requires the right point be equal or lower than the current point horizontal coordinates. In order to enhance robustness and prevent premature interruption or interference interruption matching, here relax the matching rules: peer interrupt points of no more than 2. If more than 2 will match to the right, the peer or column down vacant points should not more than 3, otherwise end the last support match. Similarly, match the lower-side hyperbolic branch and save this point set Q to array S. If the number of points in the S inner point set Q is less than the lower limit intensity threshold $T_i$, the vertex is a pseudo vertex, discard and jump to step (1), otherwise perform step (3).
3. Search a within (0, 700) and step 1, and find the corresponding parameters $y_0$ and $v$ according to Eq. (10). According to parameters $y_0$ and $v$ and Eq. (16), the corresponding $t_0$ is derived, and then the error is calculated according to Eq. (18). If the error is less than the threshold $T_p$, the error value is saved. Find the smallest error value of all the saved errors, and the corresponding parameters are the closest set of hyperbolic points, which are considered to be the desired. Go to step (2) and refit the next vertex until all point sets are finished.

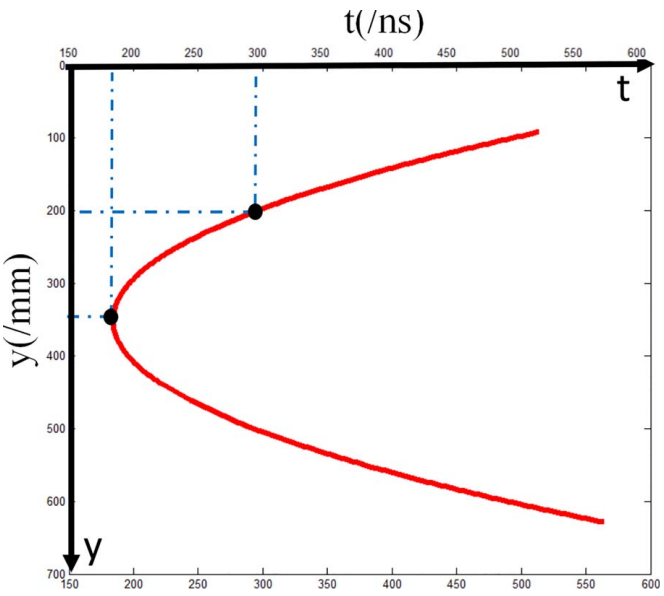


**Fig. 10.** Fitting diagram of karst cave reflection curve.

Through the above treatment, the hyperbolic fit diagram reflected by the hidden cave is shown in Fig. 10. The equation is

$$g(y) = t^2 = p_0 + p_1 y + p_2 y^2 = 429360 - 2304.5y + 3.2997y^2 \quad (21)$$

According to the relational type Eq. (11), the following can be calculated separately: $v = 0.110$ m/ns; $y_0 = 349.198$ mm; $t_0 = 164.277$ ns. According to the relational Eq. (16), if $c$ takes $2.9 \times 10^8$ m/s, $\varepsilon_r$ can be calculated, which is 7.339, whose relative dielectric constant is within the relative dielectric constant of limestone in 100 MHz electromagnetic waves, which is consistent with the actual situation. According to the relational Eq. (20), the radial size of the hidden cave can be calculated as about 624 mm, because the depth starting point selected by this example is the position of the actual drilling depth of 30 m, combined with the vertex position coordinates of the hyperbolic. It can be assumed that there is a hidden cave about 0.580 m in size at a position of about 30.349 m below the drilling ZK26 seabed, and that the hidden cave distance is about 0.75 m at the bore perimeter.

## Results Comparison

In order to verify the accuracy and reliability of the results, the results of this paper are compared with the cross-hole CT results corresponding to the drilling ZK26. The results of cross-hole CT were verified by subsequent drilling, and the results of cross-hole CT are referential and comparative. It can be seen from the cross-hole CT profile result that the drilling ZK26 peripheral geodesy structure is generally good, but there are hidden cave sites at about 30 m below the seabed, as shown in Fig. 11(a). By analyzing the panoramic drilling camera image of the drilling ZK26, as shown in Fig. 11(b), it can be seen from the drilling image that the whole section of the drilling rock wall is relatively complete, no obvious cave and crack, which verifies that the hyperbolic curve in the borehole radar image comes from the point-shaped target body of the bore hole, which is the hidden cave derived from this proposed method. By combining the cross-hole CT and drilling camera data of drilling ZK26, we can judge that the hyperbolic curve in the borehole radar signal analyzed in this paper is a hidden cave, verify the feasibility and correctness of the hidden karst cave borehole radar signal response, and provide a theoretical model basis for subsequent feature parameter extraction.

By using the subspace MUSIC method for radar signal reconstruction, the borehole radar signal one-dimensional waveform is decomposed into the useful target body, clutter, and noise three subspaces. For each signal reflection point of the exact position, the location of the reflection target is estimated by searching the peak point, as shown in Fig. 12. The peak point position of the radar signal one-dimensional waveform can reflect the reflected target state in the borehole radar image, so the image suppression obtained by subspace MUSIC method is used to reconstruct the borehole radar signal, which suppresses some interference signal, which effectively highlights the useful information.

In order to completely discard the grayscale and color variation information of the pre-processed image, it is necessary to make a borehole radar map for two-value processing. In order to verify the effect of the analysis method, a comparison of the results of its dichotomy processing with the conventional maximum interclass variance method is required. Fig. 13(a) shows the dichotomy processing of the borehole radar map using the largest interclass

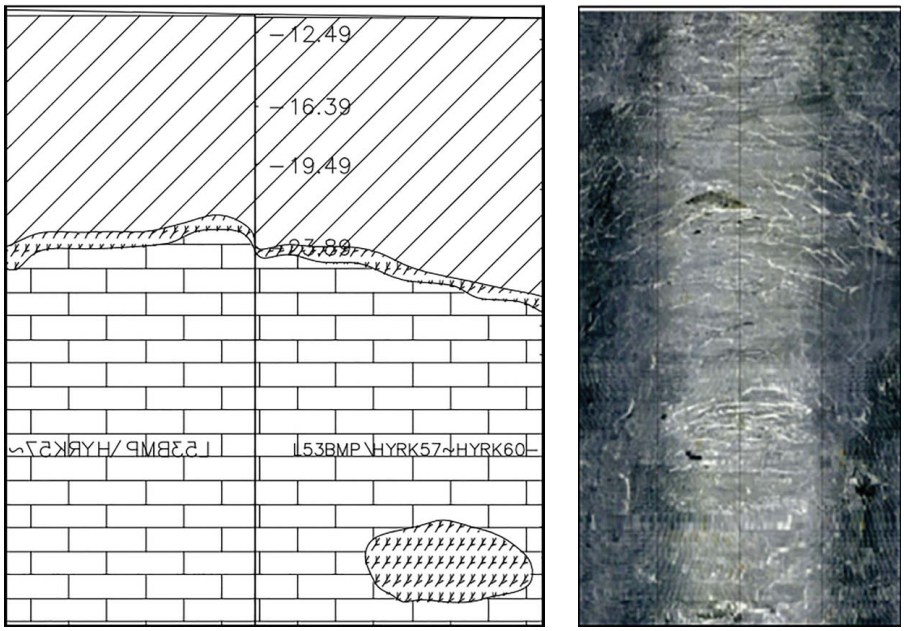


(a) (b)

**Fig. 11.** Cross-hole CT and borehole photography: (a) cross-hole CT profile; and (b) borehole camera.

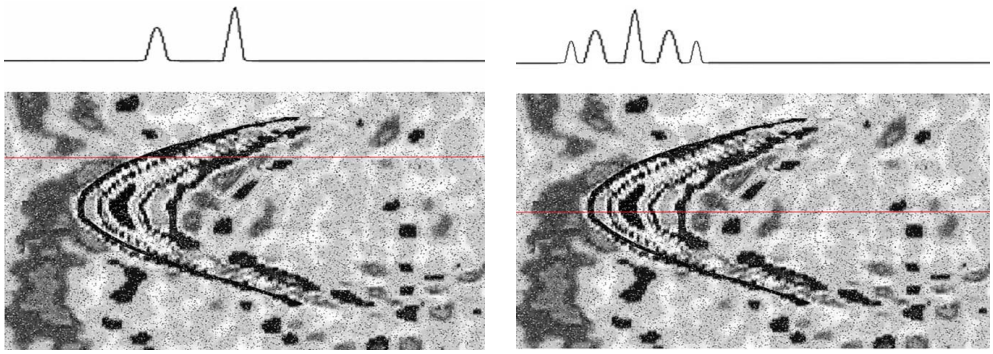

(a) (b)

**Fig. 12.** One-dimensional waveform and borehole radar: (a) article a waveform and borehole radar; and (b) article b waveform and borehole radar.

variance method. Fig. 13(b) shows the two-value processing of the borehole radar map combining the gradient operator with the largest class variance method used. It can be seen from the comparison that the two-value processing of the borehole radar map can be realized more effectively, taking into account the difference of the hidden cave reflection feature curve and the grayscale value of the nonfeatured area in the borehole radar image and discarding more invalid information.

In the realization of an image contour segmentation, this paper combines the continuity characteristics of the hyperbolic, by setting the threshold for the number of consecutive pixels. When setting the threshold value, the more redundant the information, the greater the threshold value, and the less redundant the information, and the smaller the threshold value. In this processing, the threshold value is 0.63, which can effectively avoid retaining too much contour information. In order to verify the feasibility of the image profile segmentation method, the image profile results are compared with the conventional Canny operator image profile segmentation method. Fig. 14(a) shows the image profile segmentation using the Canny operator method. Fig. 14(b) shows the image contour segmentation in this paper by setting the threshold value of the consecutive pixels number. Through the comparison, it can be seen that the image segmentation method used in this paper can achieve the suspected hidden cave reflective features of the hyperbolic contour extraction, which can avoid the effect of excessive contour information on the fit of the hidden cave hyperbolic contour.

In the metabolic equation fitting of the hidden cave, the number of image points to be detected in the image is 770,280, the number of $n$ of the hyperbolic feature points is 353 $m \ll n$, and the opening and closing degree of the hyperbole is adjusted to minimize the data error of the match (Hu and Dong 2019; Dong et al. 2019). The calculation complexity of the algorithm is much smaller than that of the normal Hough transformation detection hyperbolic, thus greatly improving the calculation efficiency and meeting the real-time calculation requirements. At the same time, the fitted curve is compared with the original feature point, and by analyzing the error rate, the margin of error is not more than ±5%. The contrasting figure is shown in Fig. 15(a).

By extracting the outline of the suspected hidden cave in the cross-hole CT at an equal interval of 10°, the 36 radius values of the vertical section of the hidden cave are obtained, and the size distribution is shown in Fig. 15(b). The average value of 36 data points is 593.976 mm, the multiple radius values obtained by fitting by the method of this paper are mainly distributed near 579.935 mm, the average value of multiple data is 634.600 mm. As can be seen from Fig. 15(b), the main distribution average of the radius value obtained by the method fitting is closer to the hidden-hole radius

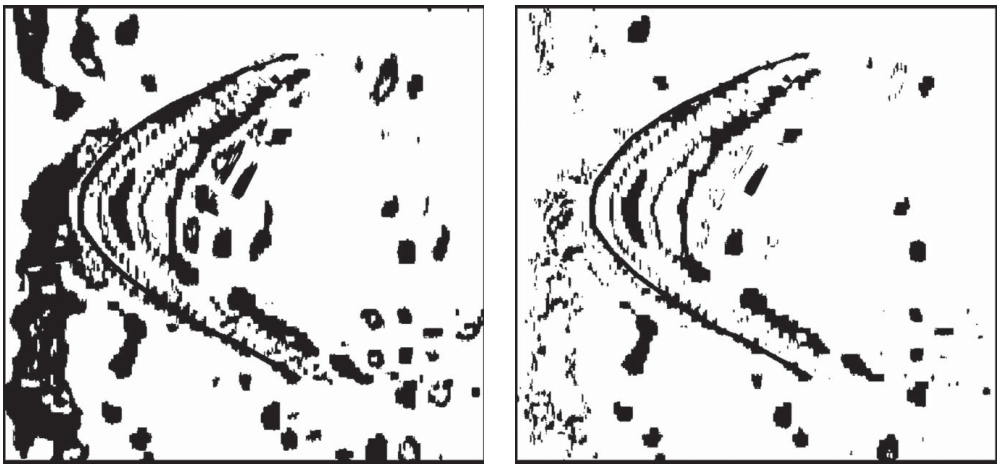

(a) (b)

**Fig. 13.** Comparison of binary processing results: (a) max-class variance processing graph; and (b) binary processing graph of this method.

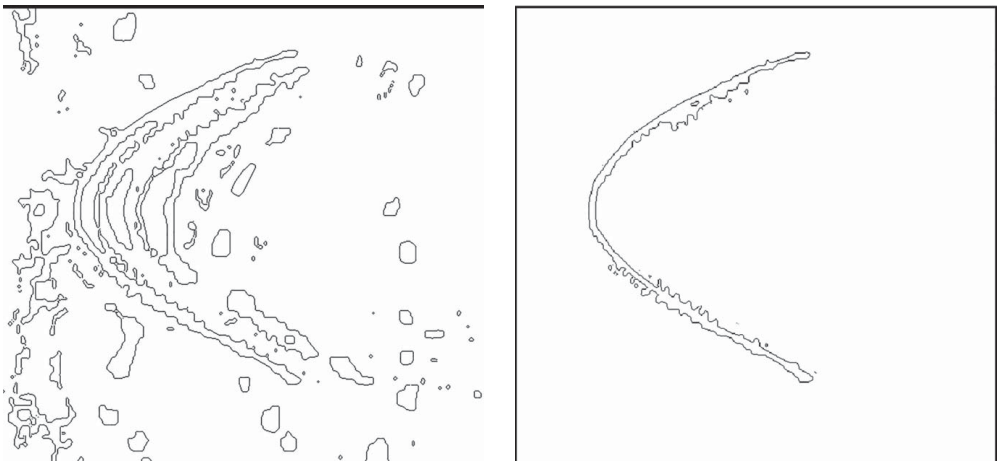

(a) (b)

**Fig. 14.** Comparison of contour extraction results: (a) canny operator contour extraction method; and (b) the contour extraction method in this paper.

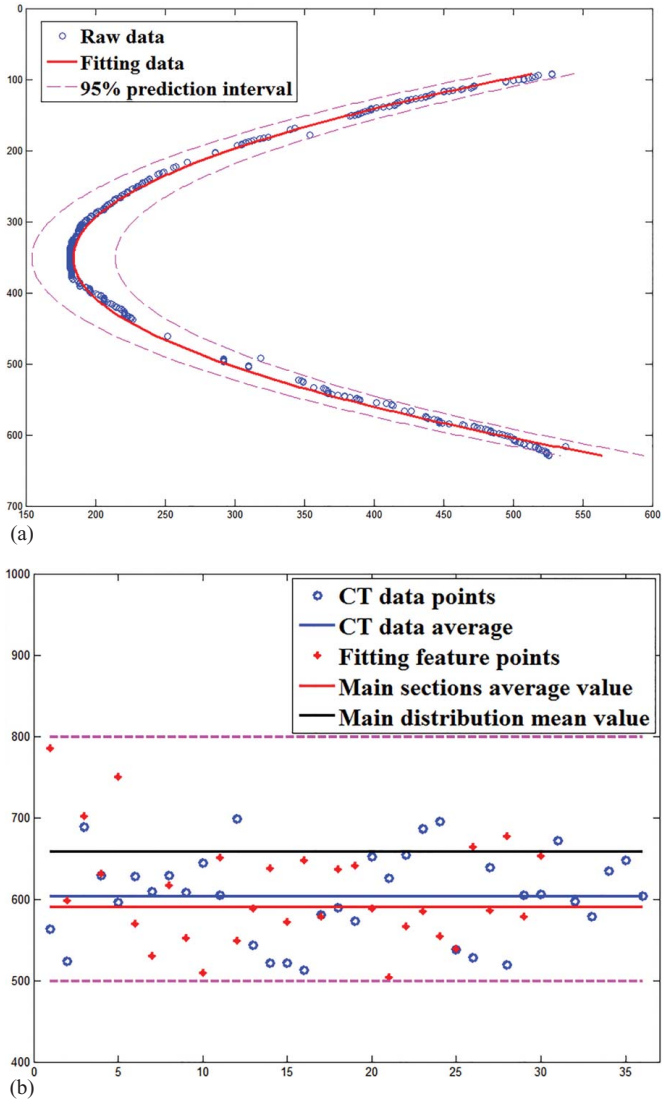


**Fig. 15.** Data comparison chart: (a) comparison of hyperbolic fitting lines; and (b) comparison of contour size data.

obtained by the cross-hole CT value, mainly due to the existence of a large number of interference and noise in the hidden cave echo The curve may appear discontinuous or render an irregular hyperbolic pattern, so that the point set ($y_i$, $t_i$) can calculate a series of radius $r_i$ values, at this time, do not take the average of these calculations as the radius of the actual hidden cave. Instead, the most dense interval of the radius $r_i$ value is used as an estimate of the size of the hidden cave. Through the calculation software, the hidden hole of the cross-hole CT is calculated far from the hole size, and the results are basically consistent with the results of the analysis method in this paper. At the same time, the dielectric normal value and average propagation speed of the rock body around the drilling obtained by the analysis method of this paper are consistent with the geological data and the actual detection environment. The feasibility and validity of this method are verified. In this paper, when analyzing the hidden karst cave, it is assumed that the karst cave is a standard circle, and the characteristic parameters extraction of hidden karst cave which is similar to a circle has a good application effect. If the hidden karst cave is not an approximate circle in the actual detection, the results of the characteristic parameters extraction need to be combined with other detection technologies and methods to achieve a comprehensive analysis.

## Conclusion

In view of the automatic recognition of hidden cave curves in an underground borehole radar and the difficulty of parameter extraction, a borehole radar detection geometry model of the hidden cave is constructed based on the original signal of borehole radar, and the reconstruction of the borehole radar signal can be realized by searching the peak point position of the Pmusic function. In order to extract the hyperbolic contour of the suspected hidden cave reflection feature, an improved variance method is proposed. Then, according to the geometric model of the borehole radar detection, an energy-weighted fitting of the hyperbolic profile is proposed, and several characteristic parameters of the improved Hough transformation method are presented to solve the hyperbolic model. Because borehole radar scanning point spacing is avoided, the three-dimensional search space is reduced to one-dimensional search space, and the computational efficiency is improved. Finally, the calculation formula of the hidden cavern characteristic parameters of borehole radar signal is deduced, and the data analysis and verification are carried out with an actual engineering case. The results show that the extraction method of the hidden cavern characteristic parameters proposed in this paper is feasible and accurate, which can provide important data support for underground engineering.

## Data Availability Statement

All data, models, and code generated or used during the study appear in the published article.

## Acknowledgments

This work was supported by the State Key Program of National Natural Science of China (Grant No. 41731284), and the National Natural Science Foundation for the Youth of China (Grant No. 41902294).

## References

Chen, D., C. Huang, and Y. Su. 2004. "An integrated method of statistical method and hough transform for GPR targets detection and location." *Acta Electron. Sinica* 32 (9): 1468–1471.

Cheng, W. C., J. C. Ni, A. Arulrajah, and H.-W. Huang et al. 2018. "A simple approach for characterising tunnel bore conditions based upon pipe-jacking data." *Tunnelling Underground Space Technol.* 71: 494–504. https://doi.org/10.1016/j.tust.2017.10.002.

Cheng, W. C., L. Wang, Z.-F. Xue, J. C. Ni, M. M. Rahman, and A. Arulrajah. 2019. "Lubrication performance of pipejacking in soft alluvial deposits." *Tunnelling Underground Space Technol.* 91: 102991. https://doi.org/10.1016/j.tust.2019.102991.

Dong, L. J., W. Zou, X. B. Li, W. W. Shu, and Z. W. Wang. 2019. "Collaborative localization method using analytical and iterative solutions for microseismic/acoustic emission sources in the rockmass structure for underground mining." *Eng. Fract. Mech.* 210: 95–112. https://doi.org/10.1016/j.engfracmech.2018.01.032.

Gurbuz, A. C., J. H. McClellan, and W. R. Scott, Jr. 2012. "Compressive sensing of underground structures using GPR." *Digital Signal Process.* 22 (1): 66–73. https://doi.org/10.1016/j.dsp.2010.11.003.

Hu, Q. C., and L. J. Dong. 2019. "Acoustic emission source location and experimental verification for two-dimensional irregular complex structure." *IEEE Sens. J.* 20 (5): 2679–2691. https://doi.org/10.1109/JSEN.2019.2954200.

Jiao, Y., W. Zhang, G. Ou, J. Zou, and G. Chen. 2019. "Review of the evolution and mitigation of the water-inrush disaster in drilling-and-blasting excavated deep-buried tunnels." *Hazard Control Tunnelling Underground Eng.* 1 (1): 36–46.

Li, H., D.-h. Wang, Y.-j. Jiao, and Y. Zhou. 2011. "Application of borehole radar technology in hydrogeology and engineering geology." *Geotech. Invest. Surv.* 39 (6): 85–89.

Li, S.-C. 2015. *The theory and method of geological prediction for the disaster source of water and mud inrush in tunnels[M]*. Beijing: China Science Publishing House.

Li, S. C., P. Lin, Z. H. Xu, L. P. Li, S. J. He, S. L. Zhao, and X. Huang et al. 2017. "Innovative method for the integral sliding stability analysis of filling media in karst caves and its applications in engineering." *Int. J. Geomech.* 17 (12): 04017109. https://doi.org/10.1061/(ASCE)GM.1943-5622.0000979.

Li, S.-C., B. Liu, H.-f. Sun, L. C. Nie, S. H. Zhong, M. X. Su, X. Li, and Z. H. Xu. 2014. "State of art and trends of advanced geological prediction in tunnel construction." *Chin. J. Rock Mech. Eng.* 33 (6): 1090–1113.

Liu, L.-b., and R.-y. Qian. 2015. "Ground penetrating radar: A critical tool in near-surface geophysics." *Chin. J. Geophys.* 58 (8): 2606–2617. https://doi.org/10.6038/cjg20150802.

Liu, S. 2002. *FDTD simulation of borehole radar and its application to electromagnetic well logging[D]*. Sendai, Japan: Tohoku Univ.

Odendaal, J. W., E. Barnard, and C. W. I. Pistorius. 1994. "Two-dimensional superresolution radar imaging using the MUSIC algorithm." *IEEE Trans. Antennas Propag.* 42 (10): 1386–1391. https://doi.org/10.1109/8.320744.

Perrotti, M., P. Lollino, N. L. Fazio, L. Pisano, G. Vessia, M. Parise, A. Fiore, and M. Luisi. 2018. "Finite element-based stability charts for underground cavities in soft calcarenites." *Int. J. Geomech.* 18 (7): 04018071. https://doi.org/10.1061/(ASCE)GM.1943-5622.0001175.

Rappaport, C. M. 2007. "Accurate determination of underground GPR wavefront and B-Scan shape from above-ground point sources." *IEEE Trans. Geosci. Remote Sens.* 45 (8): 2429–2434. https://doi.org/10.1109/TGRS.2007.901004.

Slob, E., M. Sato, and G. Olhoeft. 2010. "Surface and borehole ground-penetrating-radar developments." *Geophysics* 75 (5): 75A103–75A120. https://doi.org/10.1190/1.3480619.

Su, R., Z.-h. Zong, R.-l. Ji, W. M. Chen, J. Xu, J. Wang, and Y. H. Guo. 2007. "Application of integrated borehole measurement techniques to hydrogeological characteristics evaluation of water-conductive fault." *Chin. J. Rock Mech. Eng.* 26 (Supp. 2): 3866–3873.

Wang, J., C. Y. Wang, S. Hu, Q. Han, and Y. Wang. 2017. "Study on extraction method of structural plane parameters of borehole image." *Geotech. Mech.* 38 (10): 3074–3080.

Wu, H., Y. Jiao, H. Li, and X. Zhang. 2008. "Technical method of ground penetrating radar for detecting grouting effect of air-raid shelter and its application." *Rock Soil Mech.* 29 (Supp. 2): 307–310.

Xu, Z. H., J. Wu, S. C. Li, B. Zhang, and X. Huang. 2018. "Semianalytical solution to determine minimum safety thickness of rock resisting water inrush from filling-type karst caves." *Int. J. Geomech.* 18 (2): 04017152. https://doi.org/10.1061/(ASCE)GM.1943-5622.0001071.

Zeng, Z.-f., S.-x. Liu, and X. Feng. 2010. *The principle and application of ground penetrating radar[M]*. Beijing: Publishing House of Electronics Industry.

Zhong, S. 2008. *Borehole radar and digital camera dynamic survey technology on a number of key issues research[D]*. Beijing: Graduate School of Chinese Academy of Sciences.

Zhong, S., C. Wang, X. Tang, and Y. Liu. 2017. "Response characteristics and forward modeling of borehole radar for planar unfavorable geological bodies." *High Tech Commun.* 27 (1): 95–102.

Zhu, J. 2009. "Elliptic detection method using long axis estimation." *Comput. Syst. Appl.* 12: 79–82.